Directional quantum-controlled chemistry: Generating aligned ultracold molecules via photoassociation

S. Kallush,[1,2] J. L. Carini,[3,*] P. L. Gould,[3] and R. Kosloff[2]
[1]*Department of Physics and Optical Engineering, ORT-Braude College, P.O. Box 78, 21982 Karmiel, Israel*
[2]*The Fritz Haber Research Center, The Hebrew University of Jerusalem, Jerusalem 91904, Israel*
[3]*Department of Physics, University of Connecticut, Storrs, Connecticut 06269, USA*
(Received 21 June 2017; revised manuscript received 27 September 2017; published 10 November 2017)

Photoassociation of ultracold atoms with pulsed laser light is shown to lead to alignment of the product molecules along the excitation laser polarization axis. We theoretically investigate pulsed two-photon photoassociation of ^{87}Rb atoms into a specific weakly bound level of the $a\,^3\Sigma_u^+$ metastable electronic state and find both stationary and time-dependent field-free alignment. Although a transform-limited pulse yields significant alignment, a frequency-chirped pulse dramatically enhances the ultracold molecular formation rate at the cost of a slight decrease in the alignment. Employing multiple pulses synchronized with the vibrational and rotational periods leads to coherent enhancement of both population and alignment of the target state. Inclusion of the rotational degree of freedom in the model gives rise to processes with multiple quantum paths, which lead to quantum effects such as interference and coherence revivals.

DOI: 10.1103/PhysRevA.96.053613

I. INTRODUCTION

Quantum coherent control was conceived as a method to direct chemical reactions to a desirable outcome [1–3]. Despite the remarkable success of applying these techniques to induce unimolecular encounters such as photoisomerization [4] and photodissociation [5], the raison d'être for coherent control in the context of chemistry, namely, the assembling of multiple atoms or molecules into a new chemical species, was not realized until recently [6,7]. The main obstacle has been the preentanglement of the reactants [8]. The approach to overcome this issue differs for hot and cold collisions. For reactions in the high temperature regime ($T \gg 1$ K) [6], one has to first distill entangled pairs out of initial incoherent mixture [9]. In the cold ($T \ll 1$ K) regime [7], quantum phenomena close to threshold result in the low angular momentum states being preentangled. For the ultracold reactions and their associated slow time scales, technological developments that allow pulse shaping in the time domain [10] were used to demonstrate coherent control in ultracold photoassociation [7].

In this paper we present an aspect of quantum control unique to photochemical reactions. Such control is able to align the products of the reaction along a well-defined direction in the laboratory frame. The discipline of laboratory-frame spectroscopy of molecules is currently attracting great attention. It has emerged as a crucial element in harmonic generation [11–13], directional molecular ionization or dissociation [14,15], and other applications [16–18].

We employ here the concepts that are used to achieve alignment of already-existing molecules and adapt them into the framework of the simplest type of chemical reaction: formation of a bound molecule from two free atoms by the process of photoassociation. In addition to starting with free atoms instead of bound molecules, features arising in the system under study include the relatively slow (nanosecond) time scale of the dynamics and the adequacy of low intensities due to the resonant nature of the interaction. These time scales and intensities are similar to those employed in recent experiments [7]. Although for the sake of simplicity, the calculations presented here are for ultracold Rb samples, in principle they could be extended to any thermal regime and to a variety of species.

II. MODEL

The model describes photoassociation (PA) of two Rb atoms to synthesize an aligned Rb_2 molecule, as shown in Fig. 1(a). An ensemble of ultracold ^{87}Rb atoms is subjected to a time-dependent electric field linearly polarized along the Z axis in the laboratory frame. The shaped laser pulse is employed to associate a pair of free atoms colliding on the ground electronic state $5S_{1/2} + 5S_{1/2}$ asymptote into a bound state of the 0_g^- electronic state below the $5S_{1/2} + 5P_{3/2}$ asymptote, as shown in Fig. 1(b). Subsequently, but within the same pulse, a coherent coupling drives the excited molecule into a bound level of the $a\,^3\Sigma_u^+$ metastable state. This model extends the purely vibration-electronic system described in [7,19] by including the rotational degree of freedom.

The intermediate excited vibrational state and the pulse parameters can be optimized to yield production rates up to 10^8 molecules/s [19]. The $v' = 31$ level is chosen here as the intermediate state; therefore, the dynamics are described by the three rotational manifolds which correspond to (1) the scattering continuum of the ground electronic state, (2) the 0_g^- ($v' = 31$) intermediate electronic state, and finally (3) the next-to-last $v'' = 39$ vibrational manifold of $a\,^3\Sigma_u^+$. For all the states involved in the process, the main contribution to the excitation or deexcitation process occurs at sufficiently large internuclear distance (around $R \approx 55$ bohrs) that Hund's case (c) is applicable.

Under this assumption, the states are given by $|n J M \Omega\rangle$, where n stands for all the nonrotational quantum numbers, J is the total angular momentum, M is the projection of J on the laboratory Z axis, and Ω is the projection of J on

*Present address: 400 Main St., East Hartford, CT 06118, USA.

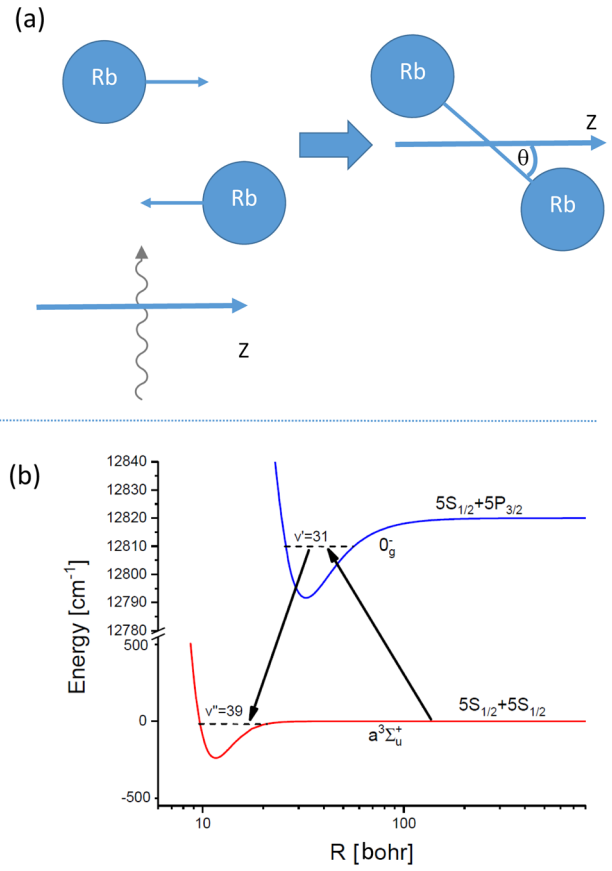

FIG. 1. (a) Schematic of the photoassociation-induced alignment. Two ultracold Rb atoms collide in the presence of photoassociation light polarized along the z axis, forming a bound molecule which exhibits a degree of alignment along z characterized by the angle θ. (b) Potential-energy curves and states involved in the two-photon photoassociation-induced alignment of Rb_2. Starting in the ground-state continuum, the photoassociation light first produces an excited molecule in the 0_g^- state, and then a weakly bound molecule in the $a\,^3\Sigma_u^+$ metastable state. Note the break in the energy scale and the logarithmic scale for internuclear separation R.

the molecule-fixed axis. Note that within Hund's case (c), the electronic orbital and spin angular momenta are not coupled to the molecular axis and therefore their projections are not separately conserved. Energies are measured relative to that of the scattering state. The Hamiltonian for the light-matter interaction has the form

$$\hat{\mathbf{H}}(t) = \hat{\mathbf{H}}_0 + \hat{\mu}\cdot\mathbf{E}(t) = \hat{\mathbf{H}}_0 + \hat{\mu}E_Z(t)\cos(\theta), \tag{1}$$

where θ is the angle between the Z axis and the molecular axis. The bound-state energies of rovibronic levels within the field-free Hamiltonian $\hat{\mathbf{H}}_0$ are given by $E_{nJ\Omega} = E_n + B_v[J(J+1) - \Omega^2]$, where E_n is the vibronic energy and $B_v = \hbar^2/2m\langle R^2\rangle$ is the level's rotational constant computed from the nuclear wave function. Due to the large outer turning points, $B_v/\hbar$ is quite small, in the 10 MHz range, indicating that the rotational dynamics will occur on the 10^{-8} s time scale. This contrasts with deeply bound molecules, e.g., $a\,^3\Sigma_u^+(v=0)$, for which $B_v/\hbar$ is in the GHz range.

The time-dependent electric-field pulse is described as

$$\mathbf{E}(t) = \hat{Z}E_0\exp[-(\sigma^{-2} + i\chi)t^2], \tag{2}$$

where E_0 is the field amplitude, σ is the temporal pulse width, and χ is the linear chirp rate. For linearly polarized light, the transition dipole moment between the different manifolds is given by

$$\langle n'J'M\Omega'|\hat{\mu}|nJM\Omega\rangle = \mu_{el}F_{nJ\Omega}^{n'J'\Omega'}\sqrt{(2J+1)(2J'+1)}(-1)^{M-\Omega} \times\begin{pmatrix} J' & 1 & J \\ M & 0 & M\end{pmatrix}\begin{pmatrix} J' & 1 & J \\ \Omega' & q & \Omega\end{pmatrix}, \tag{3}$$

where common notation is used for the Wigner $3j$ symbols, $q = -1,0,1$. μ_{el} is the electronic transition dipole moment between the states, $F_{nJ\Omega}^{n'J'\Omega'}$ are Franck-Condon (FC) factors between two vibrational levels, and $\cos(\theta) \propto D_{00}^1$, where $D_{M\Omega}^J$ is the rotational matrix wave function [20]. The FC factors are obtained using nuclear wave functions computed by a mapped Fourier grid [21,22]. The energy eigenfunctions are obtained by diagonalizing the time-independent nuclear Hamiltonian $\hat{\mathbf{H}}_{nJ\Omega} = \hat{\mathbf{T}} + \hat{\mathbf{V}}_{nJ\Omega}$, where $\hat{\mathbf{T}}$ is the kinetic-energy operator and the potential $\hat{\mathbf{V}}_{nJ\Omega}$ reads

$$\hat{\mathbf{V}}_{nJ\Omega} = V_n(R) + \frac{\hbar^2[J(J+1) - \Omega^2]}{2mR^2}, \tag{4}$$

where V_n are the Born-Oppenheimer potential curves.

The final observables such as population and alignment are obtained by solving the time-dependent Schrödinger equation for each of the initial thermal states with a given J, M, and Ω in the scattering manifold. For states with high angular momentum J, the rotational barrier in Eq. (4) induces a strong decrease of the FC overlap between the various states and eliminates transitions to and from states with $J > 5$. As was shown [23] in the ultracold regime, due to the spatial structure of the scattering wave function, a single scattering state is sufficient to represent the internuclear degree of freedom. An example of the relevant level structure for the initial level with $J = 0$ is shown in the upper right inset of Fig. 2. The observables are computed by averaging over an incoherent sum of the individual runs. Note that due to the nuclear spin statistics, the odd and even J states lead to symmetries that have to be weighted according to $P_{\rm odd}/P_{\rm even} = (I+1)/I$, where $I = 3/2$ is the nuclear spin of ^{87}Rb.

The time scales of the dynamics are comparable to the 0_g^- spontaneous decay time (22 ns). As was shown in Ref. [19], the incoherent part of the dynamics has a negligible effect on the overall PA yield. In addition, as alignment can emerge only from coherent processes, spontaneous decay cannot contribute, so we do not consider it here.

III. MOLECULAR ALIGNMENT

The molecular alignment after PA by a single transform-limited (TL) pulse, quantified by the expectation value of $\langle\cos^2\theta\rangle$, is shown in Fig. 2. The right lower inset panel presents the temporal bound-state population of the various symmetries and of the total weighted sum during the pulse. For an isotropic ensemble in thermal equilibrium, all M states for any given J are equally populated, so the probabilities to be aligned along

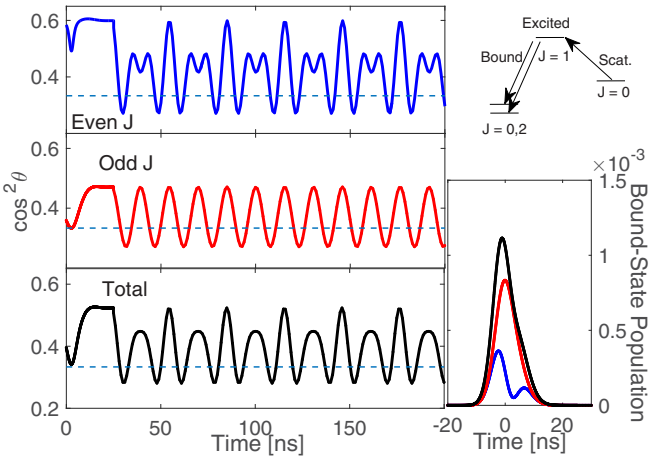

FIG. 2. Alignment of the photoassociated molecules. (Main) Alignment vs time for the even (top) and odd (middle) J states and total population (bottom). The dashed line in all the panels denotes the value of alignment for an isotropic sample. (Upper right) Rotational level scheme for the initial thermal level with $J = 0$. The full coupling scheme includes the entire set of J, M, Ω levels up to $J = 5$. (Bottom right) Bound-state population vs time for the even (blue) and odd (red) J states and the total (black). The pulse is a $\sigma = 10$ ns transform-limited pulse, with peak intensity $1000\,\mathrm{W/cm^2}$ and a detuning $\delta = 0$.

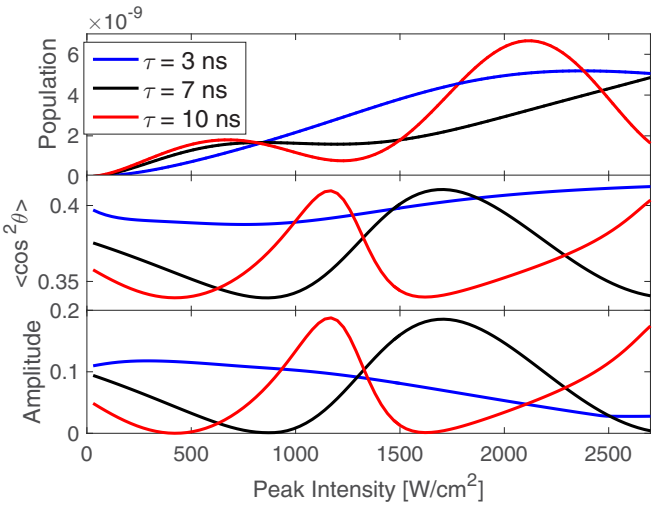

FIG. 3. Transform-limited pulses: (upper) the bound-state population, (middle) the stationary alignment, and (lower) the amplitude of the dynamic alignment, defined as half of the peak-to-peak oscillation, as functions of the peak intensity. The three curves correspond to different pulse widths.

any arbitrary direction are equal, and $\langle \cos^2\theta \rangle = 1/3$. Note that under experimental conditions that measure the alignment in a given plane, the value for an isotropic sample is $1/2$.

Two types of angular anisotropy are visible in Fig. 2. (1) The time average of the alignment is not 1/3. This indicates a stationary alignment, which results from the nonthermal population for different M states. (2) The alignment oscillates in time. This phenomena emerges from coherences between different J states with the same M value. The periodicity of the signal is found to be 30.7 ns $= 1/2B$, where B is the rotational constant of $a\,^3\Sigma_u^+(v'' = 39)$. This typical laboratory-frame alignment is the starting point of many experiments in the context of laboratory-frame spectroscopy [16].

Figure 3 shows the influence of peak intensity and pulse width on the alignment and PA yield. We note that the range of intensities shown is many orders of magnitude less than employed in ultrafast alignment experiments, and is in fact achievable with diode laser technology [24]. We also note that despite the fact that these pulses are very slow by ultrafast standards, the alignment mechanism is nonadiabatic because the pulse widths are less than the time scale of the rotational dynamics. The final bound-state populations are similar to those in our previous study [19] for TL pulses at these intensities and pulse widths. The pulses with widths $\sigma = 7$ ns and $\sigma = 10$ ns show a similar dependency of the stationary and dynamic alignment on intensity. The shorter $\sigma = 3$ ns pulse shows a different intensity dependence. Note that the binding energy of the $v'' = 39$ state is 764 MHz, which corresponds to a period of 1.3 ns. Hence, for a longer pulse, with narrow frequency bandwidth, the static and dynamic alignments emerge from the same origin, the population of the same single state, and therefore have the same behavior. This is not the case for shorter pulses, or alternatively for a chirped pulse (see below). The alignment presented in Fig. 3 under almost all of the conditions is very significant.

The field that drives the process has a well-defined polarization direction. Alignments of this magnitude should be detectable with reasonable experimental resolution. The maximum (aligned) and minimum (antialigned) values with the optimal parameters reach 0.6 and 0.2, respectively. These values depend on the number of M values that contribute to the final superposition. For ultracold PA they correspond to low J cases and $M = 0(\pm 1)$ for the most aligned (antialigned). For bulk gas-phase molecules, increasing the pulse intensity can add more M states to the superposition, leading to higher alignment. However, under ultracold initial conditions, the maximum J values achievable during PA are limited by rotational barriers and the resulting extremely sharp exponential decay of the Franck-Condon factors.

Figure 4 shows the alignment and population in the target state with a positively chirped pulse with a chirp rate $\chi = 100\,\mathrm{MHz/ns}$. As expected [7], the bound-state population here is dramatically increased, a result of the light becoming resonant with the downward transition to the bound manifold later in the pulse. Being in resonance, the population of the target bound state is maintained and not simply a transient as in the TL case in Fig. 2. Consequently, the majority of the population arrives into these states only during the later part of the pulse. The alignment here is also quite pronounced and contains the same period of 30.7 ns, but due to the population of many rotational states by the chirp, the signal here also has faster oscillations.

We have found [19] that the PA yield can be optimized by the appropriate choice of chirp parameters. The bound-state population and alignment vs chirp rate for two intensities and three pulse widths are shown in Fig. 5. The optimization of bound-state population is due to a competition between two factors. On the one hand, a slow chirp is more adiabatic and therefore more efficient. On the other hand, for a fixed pulse

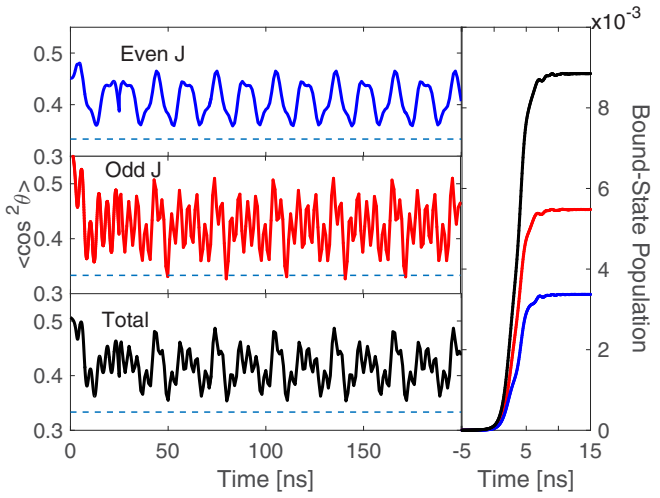

FIG. 4. Chirped pulses: similar to Fig. 2, with the same pulse width and peak intensity. The pulse is chirped at a rate of 100 MHz/ns and is on resonance with $v' = 31$ at the peak of the pulse.

width, if the chirp is too slow, the resonance for the deexcitation step is reached late in the pulse, when the intensity is low. This results in a low postpulse bound-state population, similar to the TL values shown in Fig. 3. As expected, the longer the pulse, the slower the optimizing chirp.

Due to the fact that all of the states pass through resonance at some time during the pulse, the peak intensity itself plays a minor role in the dependence of the final population on chirp rate. Because of the similar outer turning points of the two bound states, the deexcitation step in the process is easily saturated, and the bound-state population scales linearly with the field intensity. This relatively simple behavior is not maintained for the static and dynamic alignment: for low intensities the alignment is nearly the same for pulse

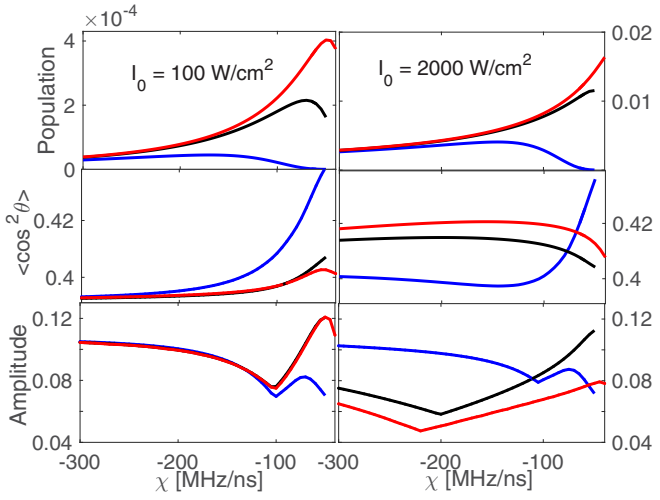

FIG. 5. Photoassociation by chirped pulses: (upper) the bound-state population, (middle) the stationary alignment, and (lower) the amplitude of the dynamic alignment as functions of the chirp rate. Left panels correspond to a peak intensity of $I_0 = 100\,\mathrm{W/cm^2}$ and right panels to $I_0 = 2000\,\mathrm{W/cm^2}$. The three curves correspond to the different pulse widths of Fig. 3.

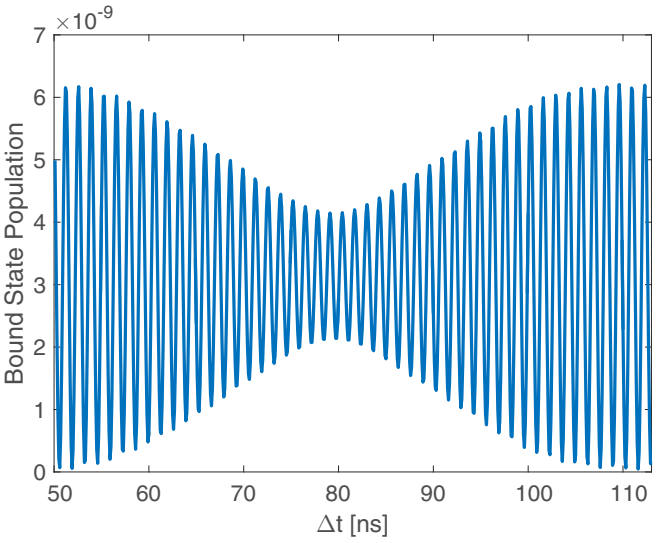

FIG. 6. Photoassociation by two pulses. Bound-state population as a function of the delay between two pulses. The pulses are 10 ns TL with $I_0 = 500\,\mathrm{W/cm^2}$.

widths above 5 ns. Once the states that are relevant for the alignment are reached during the chirp, the relative fractions of the population and their coherences are not changed, and the alignment does not depend on the pulse width. For higher intensities, interference effects start to play a role and the alignments vary significantly with respect to the various parameters. Note that due to the relatively large number of states that participate for the chirped pulses, the final static and dynamic alignment values are moderately smaller than those achieved with TL pulses. This inferior performance could probably be improved with more sophisticated manipulation of the temporal phase of the field, e.g., with the use of some formal control scheme such as local or optimal control.

In cold PA of dilute samples, coherences within a given electronic state are long lasting. As a result, a series of photoassociation pulses will add coherently to the process. The response to multiple pulses is examined in Figs. 6 and 7. The use of pulse trains is common in both ultracold PA [25] and laboratory-frame spectroscopy [26]. Figure 6 displays the bound-state population vs the time delay between the pulses. To avoid any overlap between the pulses, the minimum delay is taken to be $5\sigma = 50$ ns. Two distinct oscillation periods are visible in the graph: (I) The faster $\tau \sim 1.3$ ns period relates to the vibrational binding energy of the bound state. Note that in contrast to the conventional pulse trains that are applied to align molecules in bulk media, here newly aligned already-existing molecules are added coherently at each pulse. Thus there is a phase relation between the molecules that were created with different pulses, and interference takes place. (II) The slower time period $\tau \sim 61$ ns relates to the slower rotational energy gap of 1/B between the rotational energy states in the manifold. Note that due to the fact that the two periods are by no means commensurate, quasiperiodic dynamics occurs.

Figure 7 displays the bound-state population, the time-averaged alignment, and the dynamic alignment amplitude vs the time delay between the pulses for multiple pulses. The

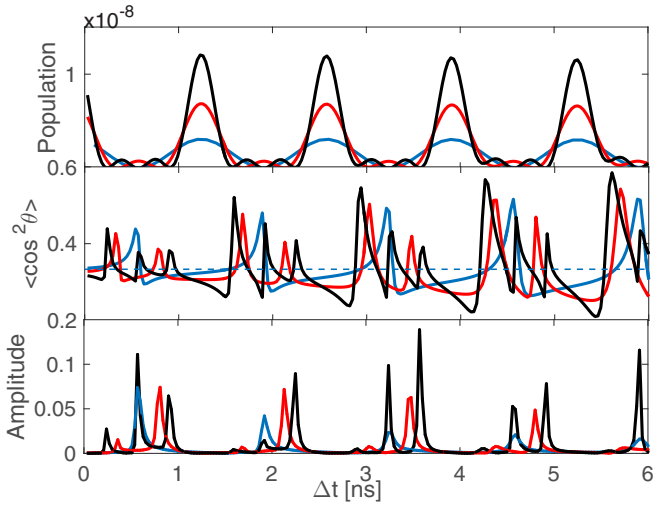

FIG. 7. Photoassociation by pulse trains: (upper) the bound-state population, (middle) the stationary alignment, and (lower) the amplitude of the dynamic alignment as functions of the delay between the pulses. The three curves at each panel are for two (blue), three (red), and four (black) pulses. The parameters for the pulses are similar to Fig. 6.

three curves correspond to the response after two, three, and four pulses.

The interference pattern of the bound-state population for n pulses resembles, for short pulse delays, the intensity pattern of n-slit interference. The patterns of the static and dynamic alignments (middle and bottom panels) show more intriguing effects: when n pulses are applied, the fundamental signal obtained for two pulses is maintained, but each peak is split into a multiplet of $n-1$ peaks whose locations are approximately symmetric about the original $n=2$ peak. Comparing the static alignment obtained after single and multiple pulses shows that the extreme values of 0.6(0.2) for the static alignment (antialignment) are obtained only under multiple-pulse conditions, taking advantage of the instantaneous phase between the bound and scattering manifolds to create interferences.

IV. DISCUSSION AND SUMMARY

In previous work [7,19,25] we have shown the ability to control the PA rates by modifying the temporal phase of the electromagnetic field. However, due to the limited bandwidth of the light compared to vibrational spacings, the matter dynamics of these examples followed a single path in phase space and thus quantum effects like interferences were not observed within this context. In this work we include the rotational degree of freedom in the model, so that the laser bandwidth is expected to cover multiple quantum paths and quantum effects such as revivals of coherences and other interference effects are predicted.

Molecular alignment of photoassociated products has never been measured directly. The prerequisite is a PA pulse which is shorter than the rotational period. The alignment of magnetoassociated ultracold molecules with respect to the magnetic field was demonstrated and examined recently [27]. A detection method should be sensitive to the alignment under the specific conditions of dilute ultracold samples. Birefringence, a common method of measuring the alignment in a bulk medium, is not appropriate due to the relatively small density of photoassociated molecules. Other approaches based on multiphoton excitation, such as Coulomb explosion [28] and harmonic generation [29], could be employed. A promising method is to extend resonance-enhanced multiphoton ionization (REMPI) that has been used for conventional PA [7] in a fashion similar to [30]. A pulse duration of a few nanoseconds should provide adequate resolution for the dynamics explored here. A linearly polarized REMPI pulse can be tuned to an electronic Π state to induce electronic excitations perpendicular to the molecule axis. For molecules which are aligned to the laboratory-fixed axis, a difference in the molecular signal for REMPI pulse polarizations parallel and perpendicular to the PA polarization should give a clear indication of the alignment. Scanning the delay of the REMPI pulse relative to the PA pulse(s) will map out the dynamics. For the alignment values presented in the current work, we can estimate the ratio of the signals to be at most on the order of $S_{\perp}/S_{||} \sim 3$. After the PA generates aligned $v'' = 39$ molecules, additional alignment can be obtained by excitation and deexcitation cycles into lower vibrational states.

The introduction of laboratory-frame spectroscopy into coherently controlled ultracold reactions raises several interesting applications. For heteronuclear ultracold molecules that possess a permanent dipole moment, controlled PA can generate macroscopic orientation of the whole ensemble. Taking advantage of the timing, this orientation can be field free. Furthermore, under BEC conditions, the induced macroscopic dipole could exhibit phenomena that originate in the quantum character of the molecules but give signatures on the macroscopic scale. A concerted rotation of the quantum condensed phase can lead to effects which will have analogs in other classical-like condensed-phase dynamics.

ACKNOWLEDGMENTS

This work is supported by the National Science Foundation through Grant No. PHY-1506244 and the US-Israel Binational Science Foundation through Grant No. 2012021. This research was supported by the Israel Science Foundation (Grant No. 510/17).

[1] D. J. Tannor and S. A. Rice, Control of selectivity of chemical reaction via control of wave packet evolution, J. Chem. Phys. **83**, 5013 (1985).

[2] D. J. Tannor, R. Kosloff, and S. A. Rice, Coherent pulse sequence induced control of selectivity of reactions: Exact quantum mechanical calculations, J. Chem. Phys. **85**, 5805 (1986).

[3] P. Brumer and M. Shapiro, Control of unimolecular reactions using coherent light, Chem. Phys. Lett. **126**, 541 (1986).

[4] V. I. Prokhorenko, A. M. Nagy, S. A. Waschuk, L. S. Brown, R. R. Birge, and R. J. Dwayne Miller, Coherent control of retinal isomerization in bacteriorhodopsin, Science **313**, 1257 (2006).

[5] M. Shapiro and P. Brumer, *Principles of the Quantum Control of Molecular Processes* (Wiley-VCH, New York, 2003), p. 250.
[6] L. Levin, W. Skomorowski, L. Rybak, R. Kosloff, C. P. Koch, and Z. Amitay, Coherent Control of Bond Making, Phys. Rev. Lett. **114**, 233003 (2015).
[7] J. L. Carini, S. Kallush, R. Kosloff, and P. L. Gould, Enhancement of Ultracold Molecule Formation Using Shaped Nanosecond Frequency Chirps, Phys. Rev. Lett. **115**, 173003 (2015).
[8] A. Abrashkevich, M. Shapiro, and P. Brumer, Coherent Control of Reactive Scattering, Phys. Rev. Lett. **81**, 3789 (1998).
[9] S. Amaran, R. Kosloff, M. Tomza, W. Skomorowski, F. Pawlowski, R. Moszynski, L. Rybak, L. Levin, Z. Amitay, M. Berglund, D. Reich, and C. Koch, Two-photon photoassociation of hot magnesium atoms by femtosecond pulses: A quantum dynamical study, J. Chem. Phys. **139**, 164124 (2013).
[10] C. E. Rogers III, M. J. Wright, J. L. Carini, J. A. Pechkis, and P. L. Gould, Generation of arbitrary frequency chirps with a fiber-based phase modulator, and self-injection-locked diode laser, J. Opt. Soc. Am. B **24**, 1249 (2007).
[11] T. Kanai, S. Minemoto, and H. Sakai, Quantum interference during high-order harmonic generation from aligned molecules, Nature (London) **435**, 470 (2005).
[12] B. K. McFarland, J. P. Farrell, P. H. Bucksbaum, and M. Gühr, High harmonic generation from multiple orbitals in N_2, Science **322**, 1232 (2008).
[13] P. M. Kraus, A. Rupenyan, and H. J. Warner, High-Harmonic Spectroscopy of Oriented OCS Molecules: Emission of Even, and Odd Harmonics, Phys. Rev. Lett. **109**, 233903 (2012).
[14] S. De, I. Znakovskaya, D. Ray, F. Anis, N. G. Johnson, I. A. Bocharova, M. Magrakvelidze, B. D. Esry, C. L. Cocke, I. V. Litvinyuk, and M. F. Kling, Field-Free Orientation of CO Molecules by Femtosecond Two-Color Laser Fields, Phys. Rev. Lett. **103**, 153002 (2009).
[15] I. V. Litvinyuk, K. F. Lee, P. W. Dooley, D. M. Rayner, D. M. Villeneuve, and P. B. Corkum, Alignment-Dependent Strong Field Ionization of Molecules, Phys. Rev. Lett. **90**, 233003 (2003).
[16] H. Stapelfeldt and T. Seideman, *Colloquium* : Aligning molecules with strong laser pulses, Rev. Mod. Phys. **75**, 543 (2003).
[17] M. Lemeshko, R. V. Krems, J. M. Doyle, and S. Kais, Manipulation of molecules with electromagnetic fields, Mol. Phys. **111**, 1648 (2013).
[18] S. Fleischer, Y. Khodorkovsky, E. Gershnabel, Y. Prior, and I. Sh. Averbukh, Manipulation of molecules with electromagnetic fields, Isr. J. Chem. **52**, 414 (2012).
[19] J. L. Carini, S. Kallush, R. Kosloff, and P. L. Gould, Efficient formation of ultracold molecules with chirped nanosecond pulses, J. Phys. Chem. A **120**, 3032 (2016).
[20] R. N. Zare, *Angular Momentum: Understanding Spatial Aspects in Chemistry and Physics* (Wiley, New York, 1988).
[21] V. Kokoouline, O. Dulieu, R. Kosloff, and F. Masnou-Seeuws, Mapped Fourier methods for long-range molecules: Application to perturbations in the $Rb_2(0_u^+)$ photoassociation spectrum, J. Chem. Phys. **110**, 9865 (1999).
[22] S. Kallush and R. Kosloff, Improved methods for mapped grids: Applied to highly excited vibrational states of diatomic molecules, Chem. Phys. Lett. **433**, 221 (2006).
[23] C. P. Koch, R. Kosloff, E. Luc-Koenig, F. Masnou-Seeuws, and A. Crubellier, Photoassociation with chirped laser pulses: calculation of the absolute number of molecules per pulse, J. Phys. B **39**, S1017 (2006).
[24] C. E. Rogers III, and P. L. Gould, Nanosecond pulse shaping at 780 nm with fiber-based electro-optical modulators, and a double-pass tapered amplifier, Opt. Express **24**, 2596 (2016).
[25] J. L. Carini, J. A. Pechkis, C. E. Rogers, P. L. Gould, S. Kallush, and R. Kosloff, Production of ultracold molecules with chirped nanosecond pulses: Evidence for coherent effects, Phys. Rev. A **87**, 011401 (2013).
[26] A. Kamalov, D. W. Broege, and P. H. Bucksbaum, Dynamical localization in molecular alignment of kicked quantum rotors, Phys. Rev. A **92**, 013409 (2015).
[27] M. Deiß, B. Drews, B. Deissler, and J. H. Denschlag, Probing the Axis Alignment of an Ultracold Spin-Polarized Rb_2 Molecule, Phys. Rev. Lett. **113**, 233004 (2014).
[28] F. Rosca-Pruna and M. J. J. Vrakking, Experimental Observation of Revival Structures in Picoseconds Laser-Induced Alignmet of I_2, Phys. Rev. Lett. **87**, 153902 (2001).
[29] L. S. Spector, M. Artamonov, S. Miyabe, T. Martinez, T. Seideman, M. Guehr, and P. H. Bucksbaum, Axis-dependence of molecular high harmonic emission in three dimensions, Nat. Commun. **5**, 3190 (2014).
[30] K. Kitano, H. Hasegawa, and Y. Ohshima, Ultrafast Angular Momentum Orientation by Linearly Polarized Laser Fields, Phys. Rev. Lett. **103**, 223002 (2009).